

Opposite translocation of long and short oligomers through a nanopore

Sebastian Getfert, Thomas Töws, and Peter Reimann
Universität Bielefeld, Fakultät für Physik, 33615 Bielefeld, Germany

We consider elongated cylindrical particles, modeling e.g. DNA fragments or nano-rods, while translocating under the action of an externally applied voltage through a solid state nanopore. Particular emphasis is put on the concomitant potential energy landscape, encountered by the particle on its passage through the pore due to the complex interplay of various electrohydrodynamic effects beyond the realm of small Debye lengths. We find that the net potential energy difference across the membrane may be of opposite sign for short and long particles of equal diameters and charge densities (e.g. oligomers). Thermal noise thus leads to biased diffusion through the pore into opposite directions. By means of an additional membrane gate electrode it is even possible to control the specific particle length at which this transport inversion occurs.

PACS numbers: 87.16.dp, 87.15.Tt, 87.15.A-

I. INTRODUCTION

The translocation of polyelectrolytes and other biomolecules through membrane pores and channels plays a prominent role in a wide variety of biological contexts, and has recently attracted much attention as a new paradigm for single molecule analysis and manipulation like DNA sequencing and other medical diagnostic applications [1]. Generally speaking, and disregarding the often quite different underlying physics, one of the most remarkable features of a pore is its selectivity regarding the permeability by different particle species [2]. In its most pronounced form, namely translocation of different particle species into opposite directions, it has been explored in much detail e.g. in the context of particle sorting by structured microfluidic channels [3].

The main objective of our present work is to extend those ideas for the purpose of separating DNA fragments, nano-rods etc. of different lengths by using a solid state nanopore. We theoretically predict the possibility of opposite translocation directions in response to an externally applied, static voltage difference across the membrane. Moreover, the specific particle length at which the transport inversion occurs can be readily modified by means of an additional membrane gate electrode. A crucial point is that all particles are assumed to exhibit the same diameter and the same charge density (per lengths unit or per surface area unit). It is only the particle length which may differ and which then may result in opposite translocation directions through the pore. In other words, given a particle of suitable length, after breaking that particle into two equal pieces, those two pieces will move through the pore in the opposite direction than the original, long particle.

A typical set-up we have in mind is sketched in Fig. 1. Such systems are governed by a complex and often quite non-intuitive interplay of various electrohydrodynamic effects [4–7], which are mainly rooted in the electric double layers at the membrane and particle surfaces due to certain, approximately constant surface charge densities σ_m and σ_p , respectively [8–11]: These charged

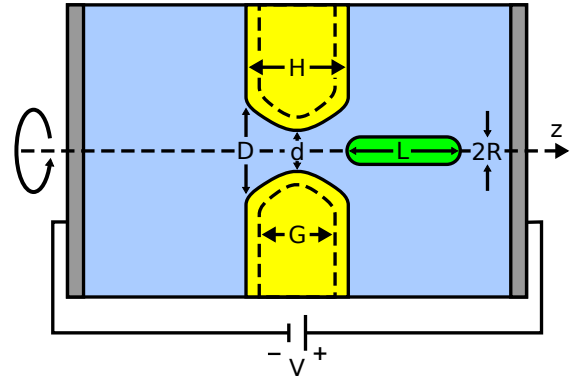


FIG. 1: (Color online) Schematic illustration of the system. A membrane of thickness H (yellow) separates two compartments with electrolyte solution (blue) and contains an hourglass-shaped nanopore with minimal and maximal diameters d and D [17]. The dashed lines indicate the possibility of an additional gate electrode of thickness G , as considered later in the paper. A voltage V is applied to the electrodes (gray) and acts on a prolate particle with radius R and length L (green). The system is symmetric about the z -axis and z denotes the distance between pore and particle center.

surfaces attract counterions (and repel coions) of the ambient electrolyte, resulting in a Debye screening layer of width λ_D [12]. An externally applied voltage generates forces on all those fixed and mobile charges and thus leads to an electroosmotic fluid flow superimposed by an electrophoretic motion of a “free” particle, or to equivalent hydrodynamic and electrostatic forces on an immobilized particle [6, 11, 13]. Since the membrane is insulating, nearly the entire voltage drop and the hence induced forces actually occur in the nanopore and its immediate neighborhood [4, 5, 11].

In the next section we will provide an intuitive picture of the main physical mechanisms governing those forces. Subsequently, we will turn to a quantitative illustration based on the Poisson, Nernst-Planck, and Stokes equations (Sects. III and IV). Generalizations of the model,

in particular the effects of an additional membrane gate electrode (dashed line in Fig. 1), are covered by Sect. V. Our summary and conclusions are provided by Sect. VI.

II. QUALITATIVE CONSIDERATIONS

We first focus on thin Debye layers [14], i.e. λ_D is much smaller than the distance between perforated membrane and immobilized particle, and also much smaller than any curvature-radii of their charged surfaces (cf. Fig. 1). Disregarding for a moment those thin Debye layers, the remnant “outer region” of the electrolyte solution exhibits the following “similitude” property [15]: Whatever the electric field in the system from Fig. 1 will look like, the concomitant electroosmotic velocity field will be proportional to this electric field throughout the outer region, provided that membrane and particle exhibit identical zeta-potentials. In our present case of thin Debye layers, the latter condition is tantamount to identical surface charge densities, i.e. $\sigma_m = \sigma_p$ [12]. This similitude property of the outer region can be complemented by means of matched asymptotic expansion techniques with explicit solutions for the electric and fluid flow fields within the thin Debye layers [15]. The result is an exact cancellation of the hydrodynamic and electrostatic forces on any charged surface element. We thus arrive at the quite remarkable conclusion that no net force (nor torque) is acting on the particle in Fig. 1 for equal surface charge densities ($\sigma_m = \sigma_p$) and asymptotically small Debye lengths λ_D , independently of the external trans-membrane voltage and any further details (shape, layout, material) of membrane, pore, and particle!

What happens beyond thin Debye layers? First of all, constant zeta-potentials are then no longer tantamount to constant surface charge densities. In particular, the zeta-potentials now depend, amongst others, on the surface curvatures and the distance between particle and membrane [12, 16]. Henceforth, we thus adopt the latter, physically more natural assumption of (approximately) constant surface charge densities $\sigma_m = \sigma_p$ [9, 19].

In a first step, we consider a spherical particle of radius R in the above special case $\sigma_m = \sigma_p$ and $R \gg \lambda_D$. How will the concomitant cancellation of hydrodynamic and electrostatic forces be modified as R decreases? In the opposite limit $R \ll \lambda_D$ there are negligibly few ions within the hydrodynamically relevant neighborhood of the particle [12], and thus the electrostatic force equals charge $4\pi\sigma_p R^2$ times electric field, while the hydrodynamic force equals Stokes friction $6\pi\eta R$ (η being the fluid viscosity) times fluid velocity (caused by electroosmosis). Due to the R^2 decay, the former becomes negligible as $R \rightarrow 0$. It is furthermore quite plausible that the same trend sets in as soon as R becomes comparable or smaller than λ_D , i.e. the particle will be dragged into the direction of the electroosmotic flow. In the most common case of negative surface charges [9, 19], this direction is from right to left for the voltage sign convention of Fig. 1.

Analogous conclusions readily carry over to arbitrary particle shapes upon observing that when scaling down its size by a factor α , the surface and hence the charge decrease as α^2 , whereas the Stokes friction decreases as α . However, while for spheres the predominance of electroosmosis sets in at $R \approx \lambda_D$, the corresponding threshold will now depend on the detailed particle shape. E.g. for a cylindrical rod, whose radius R is much smaller than its length L , the threshold is at $L \approx \lambda_D$ [20]. For Debye lengths comparable to R we thus expect that spheres and short rods are dragged by electroosmosis from right to left in Fig. 1, while the net force on long rods is still negligible.

So far, we tacitly ignored any spatial variations of the electric and fluid flow fields over the particle-length L , as well as any back-coupling of the particle to those fields. To better understand those finite particle size effects, we now turn to another simple limiting case, namely $\lambda_D \rightarrow \infty$. As expected [14], the system then behaves essentially as in the absence of any ions: Electroosmosis is negligible, and upon entering the pore, the particle is strongly repelled by the hardly screened like-charges of the membrane, and symmetrically when exiting the pore. From the energetic viewpoint, the corresponding two energy barriers thus nearly cancel each other so that there still remains a net potential energy gain when a negatively charged particles moves from the left to the right fluid compartment in the presence of a voltage with the sign convention from Fig. 1. Upon gradually reducing the Debye length, the potential barriers as well as the net energy gain for left-to-right translocations will clearly decrease, but it is also quite plausible that we may still encounter remnants of both effects down to quite small Debye lengths: The barriers may then also be viewed as due to the “bumping” of the counterion cloud (Debye layer) around the particle into that around the membrane, and the overall predominance of the electrostatic (from left to right) over the hydrodynamic forces (from right to left) may be viewed as due to the fact that a merging of the counterion clouds reduces the number of counterions in regions with high external fields and thus the fluid flow which they induce. Finally, it is also quite clear that for any given Debye length, both effects (energy barriers and predominance of electrostatic forces) will become weaker and weaker as the particle size decreases.

Altogether, we thus predict that for $\sigma_m \approx \sigma_p$, $\lambda_D \approx R$, and pore diameters of a few R , there will be a competition between the two above mentioned effects, the first prevailing for short and the second for long rods. Hence, the potential energy difference across the same pore will be of opposite sign for long and short rods.

III. NUMERICAL TREATMENT

To quantitatively verify our above predictions, we consider the system from Fig. 1 with a cylindrical fluid

chamber, a planar, solid state membrane of thickness $H = 20$ nm, surface charge density $\sigma_m = -50$ mC/m² [9, 19], and an hourglass-shaped pore with $d = 10$ nm and $D = 20$ nm [17]. The electrolyte's temperature and viscosity are $T = 300$ K and $\eta = 10^{-3}$ Pa s, and we assume two ionic species with opposite charges $q_1 = -q_2 = e = 1.6 \dots \cdot 10^{-19}$ C, equal thermal diffusion coefficients $D_1 = D_2 = 2 \cdot 10^{-9}$ m²/s, and equal bulk concentrations $c_0 = 100$ mM [21]. Accordingly, the Debye length is $\lambda_D \approx 1$ nm [12]. The cylindrical particle of radius R and length $L \geq 2R$ (cf. Fig. 1) exhibits spherical caps and becomes a sphere for $L = 2R$. Besides actual nano-rods, we mainly have in mind fragments of a polyelectrolyte (e.g. DNA) which are sufficiently short (oligomers) that our rigid particle remains a reasonable approximation [9, 13, 22]. In the same vein, we approximate the real particle charges by a constant surface charge density σ_p [8, 11, 23]. Henceforth, we specifically focus on the radius $R = 1.1$ nm of double stranded DNA and lengths L between $2R$ and 50 nm. Given a DNA basepair-distance of about 0.3 nm, a nominal charge of $-2e$ per basepair, and a typical screening factor of about 60% due to counterion adhesion (transient binding) [6–9, 24, 25], the equivalent surface charge density $\sigma_p \approx -50$ mC/m² is quite similar to σ_m . Since equal particle and membrane surface charges densities also represents the conceptually most interesting situation, we first focus on this case.

Polarization effects within the electrolyte solution are taken into account via its dielectric constant (permittivity) ϵ_s [26], and likewise for membrane (ϵ_m) and particle (ϵ_p). Under the name “self-energy” they play a key role e.g. in narrow protein channels [5, 27], while for our present, much larger pores they are expected to be of minor importance [13]. We usually set $\epsilon_s = 80\epsilon_0$, $\epsilon_m = \epsilon_p = 5\epsilon_0$, where ϵ_0 is the vacuum permittivity, and we verified that variations of ϵ_m and ϵ_p between ϵ_0 and ϵ_s indeed only lead to minor changes e.g. in Figs. 2–5 [28].

Next we turn to the Poisson, Nernst-Planck, and Stokes equations, which are well-established in this context [21, 29, 30], and thus only briefly summarized here. Throughout the electrolyte solution the electric potential ψ satisfies Poisson's equation $\epsilon_s \Delta \psi(\mathbf{x}) = -\rho(\mathbf{x})$, where $\rho(\mathbf{x}) = F_c [c_1(\mathbf{x}) - c_2(\mathbf{x})]$ is the charge density in terms of Faraday's constant F_c and the molar concentrations $c_{1,2}(\mathbf{x})$ of the two ionic species (see above). Likewise, $\Delta \psi(\mathbf{x}) = 0$ throughout the perforated membrane and the particle. Boundary conditions are $\psi = \pm V/2$ at the electrodes and $\mathbf{n} \nabla \psi = 0$ at the cylindrical chamber walls (cf. Fig. 1), where \mathbf{n} indicates the surface normal. At the charged liquid-membrane interface we require that $\mathbf{n}[\epsilon_s \mathbf{E}_s - \epsilon_m \mathbf{E}_m] = \sigma_m$ where \mathbf{E}_s and \mathbf{E}_m are the electric fields $-\nabla \psi$ at the two sides of the interface [13, 16, 22, 26], and analogously at the particle-liquid interface.

According to Nernst-Planck, the flux densities \mathbf{J}_ν of the two ionic species ($\nu = 1, 2$) are given by $c_\nu(\mathbf{x})\mathbf{u}(\mathbf{x}) - D_\nu \nabla c_\nu(\mathbf{x}) - \mu_\nu c_\nu(\mathbf{x}) \nabla \psi(\mathbf{x})$, where \mathbf{u} is the fluid velocity,

$\mu_\nu := q_\nu D_\nu / k_B T$ the ion mobility, and k_B Boltzmann's constant, and they satisfy $\nabla \cdot \mathbf{J}_\nu(\mathbf{x}) = 0$. At the electrodes, the concentrations c_ν must assume their bulk value c_0 . On all other boundaries we impose $\mathbf{n} \cdot \mathbf{J}_\nu = 0$.

The velocity \mathbf{u} and pressure p satisfy Stokes equation $\eta \Delta \mathbf{u}(\mathbf{x}) = \nabla p(\mathbf{x}) + \rho(\mathbf{x}) \nabla \psi(\mathbf{x})$ and $\nabla \cdot \mathbf{u}(\mathbf{x}) = 0$ with no-slip boundary conditions $\mathbf{u} = \mathbf{0}$ on membrane, particle, and cylindrical chamber walls. At the electrodes we require: (i) The pressure p assumes a preset “bulk value”, whose actual choice turns out to be irrelevant. (ii) The hydrodynamic stress tensor A with matrix elements $A_{ij} := \eta(\partial u_i / \partial x_j + \partial u_j / \partial x_i) - p \delta_{ij}$ satisfies $A \mathbf{n} = \mathbf{0}$. These boundary conditions are well-known to be numerically very efficient and stable [30].

Finally, the force \mathbf{F} on the particle is obtained as the integral $\int_S [A(\mathbf{x}) + B(\mathbf{x})] \mathbf{n}(\mathbf{x}) dS$ over the particle surface S [30], where B is the Maxwell stress tensor with matrix elements $B_{ij} := \epsilon_s (E_i E_j - \delta_{ij} |\mathbf{E}|^2 / 2)$ and $\mathbf{E} := -\nabla \psi$. Focusing on particle positions along the z -axis (cf. Fig. 1), we denote by z the distance between pore- and particle-center, and by $F(z)$ the z -component of \mathbf{F} . The potential energy $U(z)$ then follows by integrating $-F(z)$ and setting $U(z) = 0$ when the particle touches the left electrode in Fig. 1.

Below, we present numerical results for $U(z)$ obtained along these lines with the COMSOL 4.3a finite element package of coupled partial differential equation solvers [31]. We tested the numerics by verifying our above mentioned prediction that $U(z) \equiv 0$ for $\lambda_D \rightarrow 0$ [14]. Furthermore, we made sure that finite-size effects of the fluid chamber in Fig. 1 remain negligible by choosing a diameter of 200 nm and a length of 400 nm.

IV. RESULTS

Without external voltage, Fig. 2 shows results for the above specified parameter values. As expected, upon entering the pore from either side, the particles encounter potential barriers, which decrease for smaller particles and increase with increasing Debye length λ_D [14]. The “plateau” of $U(z)$ for $L = 50$ nm is due to an approximate translation invariance when both rod-ends stick far out of the pore [33]. Accordingly, one finds that for even longer rods the width of the plateau grows, while its height and the shape of the “potential steps” at its edges hardly change.

Typical results for finite voltage are depicted in Fig. 3: [32]: Very roughly speaking, the barriers from Fig. 2 get “tilted” by the external voltage. However, this “tilt” is very different for different particle lengths, and neither spatially homogeneous nor symmetric about $z = 0$. Only for $L = 50$ nm, a region with constant slope develops around $z = 0$, analogous to the “plateau” in Fig. 2 [33]. Moreover, the potentials $U(z)$ approach their large- z limits much slower than in Fig. 2 and in agreement with the $1/|z|$ asymptotics of ψ predicted in [4]. Most importantly,

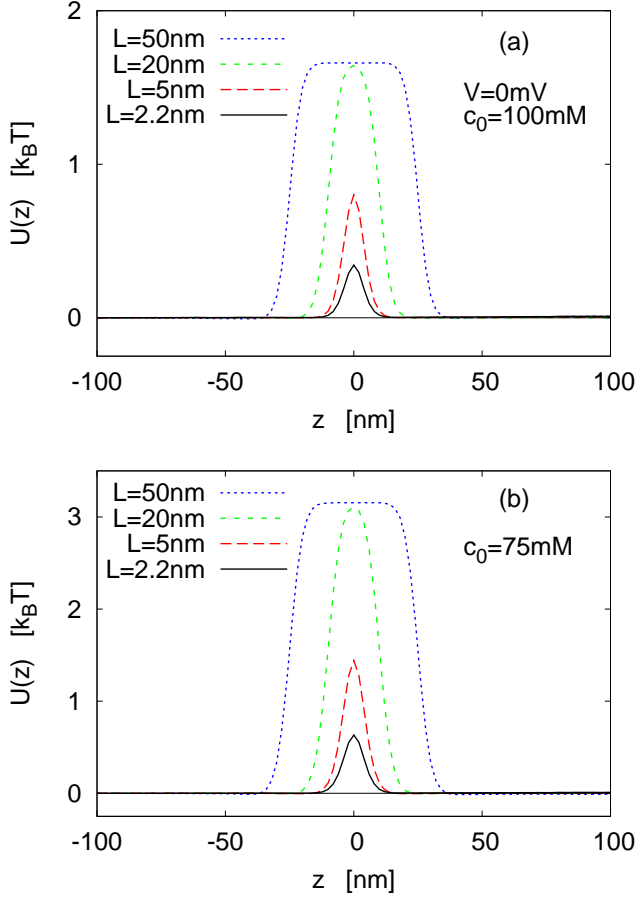


FIG. 2: (Color online) The potential energy $U(z)$ in units of the thermal energy $k_B T$ of a particle at position z (in units of nm; cf. Fig. 1) for different particle lengths L , $V = 0$ mV, $c_0 = 100$ mM, and $\sigma_m = \sigma_p = -50$ mC/m². (a): Bulk concentration $c_0 = 100$ mM. (b): Reduced bulk concentration $c_0 = 75$ mM.

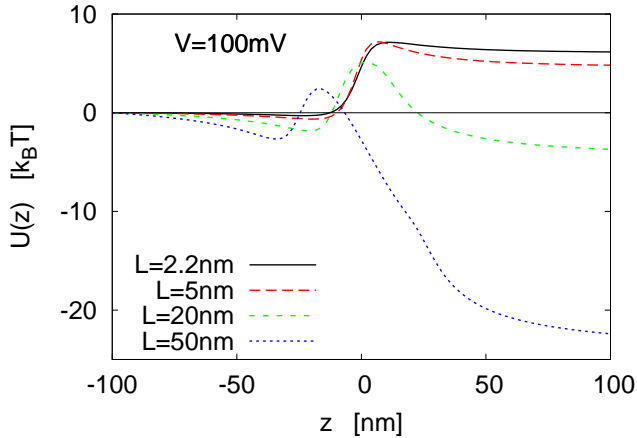


FIG. 3: (Color online) Same as in Fig. 2(a) ($c_0 = 100$ mM, $\sigma_m = \sigma_p = -50$ mC/m²) but now for an externally applied voltage of $V = 100$ mV.

the potential energy difference $U(z) - U(-z)$ for large z is indeed of opposite sign for short and long particles, and also the signs themselves agree with our predictions from Sect. II.

Note that $U(z)$ in Fig. 3 is not monotonically decreasing (increasing) for long (short) rods. However, the intermediate potential barriers of a few $k_B T$ are readily surmountable by thermal noise. We remark that higher voltages V lead to larger potential energy differences [32] and hence a better selectivity of the pore, but also the barriers become less easy to surmount.

Since the externally applied voltage drop V mainly occurs within and close to the pore (see above and end of Sect. I), the concomitant “purely electrostatic” transmembrane potential energy difference follows as qV , where q is the total particle charge, i.e. the net particle surface times its surface charge density. The actual potential energy differences in Fig. 3, i.e. $U(z) - U(-z)$ for $z \geq 100$ nm, is considerably smaller than qV for the long particles ($L = 50$ nm and $L = 20$ nm) and even of opposite sign for the short particles. The main reason for those differences are clearly the electroosmotic forces (cf. Sect. II), which in fact would exert forces even when the particles were not charged at all (i.e. $qV = 0$).

Finally, the electric and hydrodynamic force contributions to the net potentials from Fig. 3 are exemplified by Fig. 4. As detailed at the beginning of Sect. III, for asymptotically small Debye lengths, those two partial forces cancel exactly. Accordingly, going beyond small Debye lengths is essential to obtain non-vanishing net forces (and potentials). Yet, our Debye lengths are still so small that the two partial forces remain quite similar in modulus but of opposite sign in Fig. 4. In other words, they still almost cancel each other and the resulting net force is much smaller than each partial force. Note that while the forces in Fig. 4 are only slightly asymmetric about $z = 0$, the hence resulting asymmetry of the potentials in Fig. 3 is more pronounced.

V. EXTENSIONS

As a first generalization, we turn to unequally charged particle and membrane surfaces, say $\sigma_p = -50$ mC/m² and $\sigma_m = -40$ mC/m². For small Debye lengths λ_D [14], the above mentioned similitude argument thus breaks down. Rather, since $|\sigma_p| > |\sigma_m|$, the hydrodynamic forces are now overwhelmed by the electrostatic forces, i.e. all particles move preferentially from left to right in Fig. 1. Analogous modifications are expected for moderate Debye lengths. This is confirmed by Fig. 5, whose main difference from Fig. 3 is an additional “tilt to the right”. Similarly, one finds that upon further increasing σ_m , this “tilt to the right” grows, and above about -10 mC/m² all particles move preferentially from left to right. Analogous effects are recovered for $\sigma_m < \sigma_p$ and upon variation of σ_p at fixed σ_m .

Finally, we will show that practically the same effects

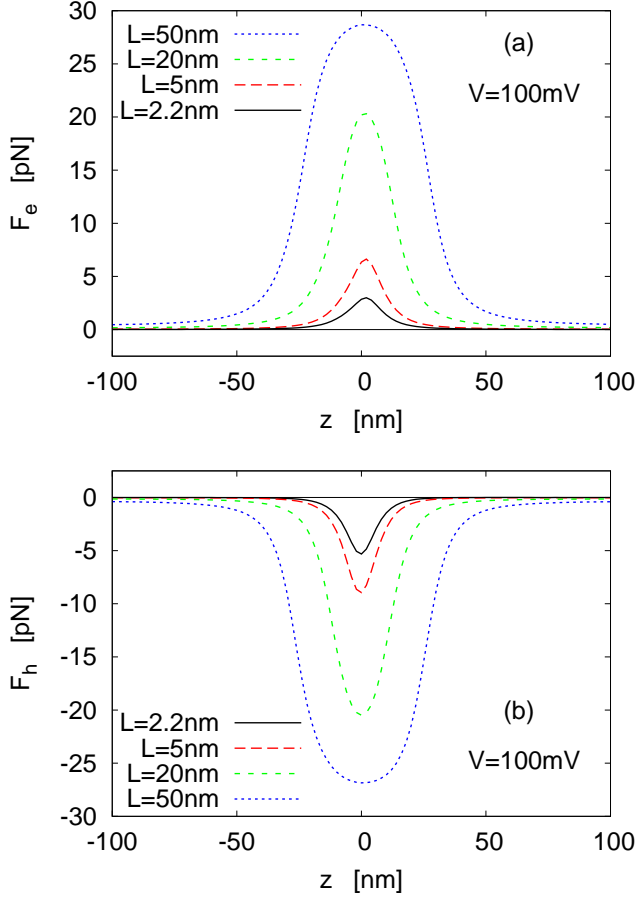


FIG. 4: (Color online) The two partial forces $F_e(z)$ and $F_h(z)$ in units of pN versus z in units of nm, obtained (as detailed at the end of Sect. III) by integration of the Maxwell and hydrodynamic stress tensors over the particle surface, respectively, for the same system as in Fig. 3. In other words, the potentials $U(z)$ from Fig. 3 are recovered upon integration of $-F_e(z) - F_h(z)$.

as by changing σ_m can be generated by a membrane gate voltage. Similarly as in Refs. [9, 22, 34], a gate electrode of thickness G is integrated into the membrane (dashed lines in Fig. 1), and is thus still coated by a non-conducting layer of thickness $h := (H - G)/2$. The applied voltage V_{gate} fixes the electric potential ψ of the gate electrode relatively to the potentials $\psi = \pm V/2$ of the external electrodes. In the absence of the pore, one can analytically show that a gate voltage V_{gate} is approximately equivalent to changing the “bare” membrane surface charge density σ_m by $\Delta\sigma_m \approx \epsilon_m V_{gate}/h$. Numerically, we found that this equivalence remains valid in remarkably good approximation even in the presence of the pore. For instance, for the system resulting in Fig. 3, an additional membrane gate electrode with $h = 2$ nm and $V_{gate} = 500$ mV amounts to $\Delta\sigma_m \approx 10$ mC/m², and indeed reproduces the dotted lines quite well.

The most important consequence of this observation

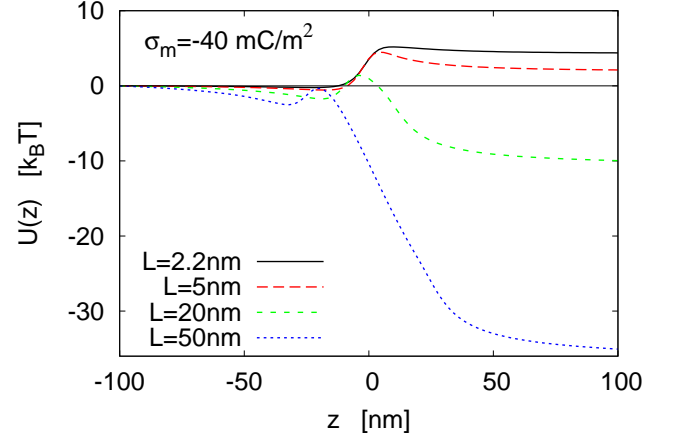


FIG. 5: (Color online) Same as in Fig. 3 ($V = 100$ mV, $c_0 = 100$ mM) but now for an increased membrane surface charge density of $\sigma_m = -40$ mC/m².

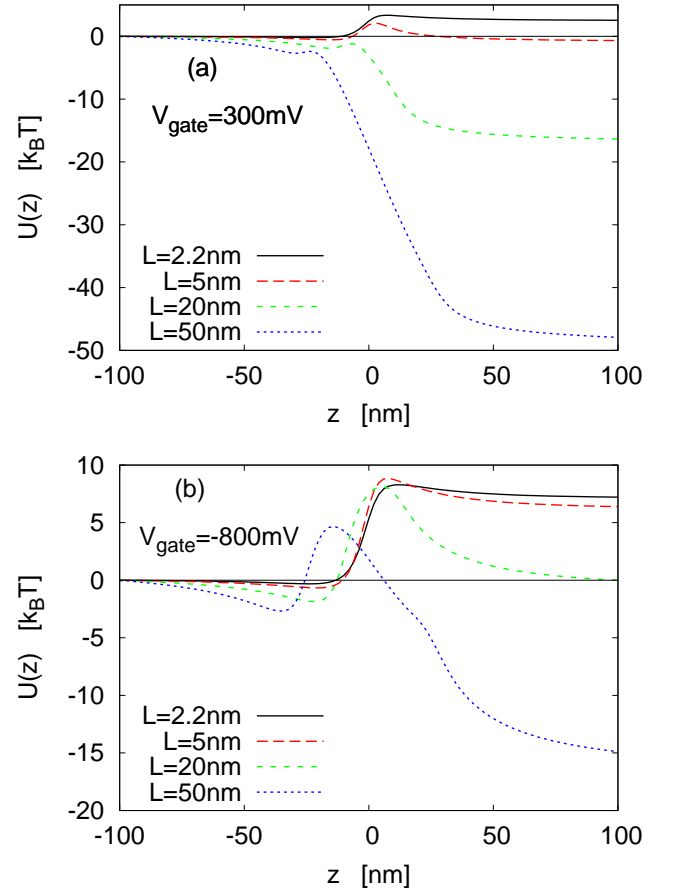


FIG. 6: (Color online) Same as in Fig. 5 ($V = 100$ mV, $c_0 = 100$ mM, $\sigma_m = -40$ mC/m²) but now for an additional membrane gate electrode of thickness $G = 16$ nm (see Fig. 1) with gate voltage $V_{gate} = 300$ mV (a) and $V_{gate} = -800$ mV (b).

is illustrated by Fig. 6, namely that the threshold-length, above and below which particles preferentially move into opposite directions, is at about $L = 5$ nm for $V_{gate} = 300$ mV and can be moved to about $L = 20$ nm by decreasing the gate voltage to $V_{gate} = -800$ mV. As expected, one finds that also a large variety of other threshold-lengths can be realized by suitably choosing V_{gate} , and that analogous results are recovered also for other values of the surface charges σ_p and σ_m than in Fig. 6.

VI. SUMMARY AND CONCLUSIONS

In conclusion, we have shown that the interplay of hydrodynamic and electrostatic forces beyond the realm of small Debye lengths gives rise to quite non-trivial potential energy landscapes, which an elongated cylindrical particle encounters while translocating under the action of an externally applied voltage through a solid state nanopore. In particular, the net potential energy difference across the membrane may be of opposite sign for short and long particles of constant diameter and charge density, for instance DNA-fragments (oligomers)

or nano-rods. Thermal noise thus leads to biased diffusion through the pore into opposite directions. By means of an additional membrane gate electrode it is even possible to control the specific particle length, above and below which the preferential pore passage occurs into opposite directions.

This new particle sorting concept seems to us quite worthwhile and feasible by today's solid state nanopore techniques [1, 34]. While the considered setup (Fig. 1) and its quantitative treatment (Poisson, Nernst-Planck, and Stokes equations) admittedly neglect many details of real systems, we believe that our approach still captures the essential features quite faithfully.

In other words, the predicted opposite translocation of long and short DNA fragments or nano-rods through a solid state nanopore, and its control by a gate electrode seem generic within a wide range of typical experimental conditions. Applications e.g. for particle sorting purposes are immediate, and by employing many pores in parallel or in series, throughput as well as selectivity can be readily enhanced [2, 3].

This work was supported by Deutsche Forschungsgemeinschaft under SFB 613 and RE1344/8-1.

-
- [1] A. Meller, J. Phys.: Condens. Matter **15**, R581 (2003); C. Dekker, Nat. Nanotech. **2**, 209 (2007); D. Branton et al., Nat. Nanotech. **26**, 1146 (2008); M. Zwolak and M. Di Ventra, Rev. Mod. Phys. **80**, 141 (2008); B. M. Venkatesan and R. Bashir, Nat. Nanotech. **6**, 615 (2011)
 - [2] R. S. Shaw, N. Packard, M. Schröter, and H. L. Swinney, PNAS **104**, 9580 (2007); S. M. Iqbal, D. Akin, and R. Bashir, Nat. Nanotech. **2**, 243 (2007); D. Goulding, J.-P. Hansen, and S. Melchionna, Phys. Rev. Lett. **85**, 1132 (2000)
 - [3] C. Marquet, A. Buguin, L. Talini, and P. Silberzan, Phys. Rev. Lett. **88**, 168301 (2002); S. Matthias and F. Müller, Nature **424**, 53 (2003); G. Mahmud et al., Nat. Phys. **5**, 606 (2009)
 - [4] A. Y. Grosberg and Y. Rabin, J. Chem. Phys. **133**, 165102 (2010); M. Wanunu, W. Morrison, Y. Rabin, A. Y. Grosberg, and A. Meller, Nat. Nanotechnol. **5**, 160 (2010)
 - [5] J. Zhang and B. I. Shklovskii, Phys. Rev. E **75**, 021906 (2007);
 - [6] B. Luan and A. Aksimentiev, Phys. Rev. E **78**, 021912 (2008)
 - [7] Y. Rabin and M. Tanaka, Phys. Rev. Lett. **94**, 148103 (2005)
 - [8] S. Ghosal, Phys. Rev. Lett. **98**, 238104 (2007)
 - [9] Y. He, M. Tsutsui, C. Fan, M. Taniguchi, and T. Kawai, ACS Nano **5**, 5509 (2011)
 - [10] R. M. M. Smeets, U. F. Keyser, D. Krapf, M.-Y. Wu, N. H. Dekker, and C. Dekker, Nano Lett. **6**, 89 (2006); H. Chang, F. Kosari, G. Andreadakis, M. A. Alam, G. Vasmatazis, and R. Bashir, Nano. Lett. **4**, 1551 (2004)
 - [11] S. van Dorp, U. F. Keyser, N. H. Dekker, C. Dekker, and S. G. Lemay, Nat. Physics **5**, 347 (2009)
 - [12] H. Bruus, *Theoretical Microfluidics*, Oxford Univ. Press (2008)
 - [13] S. Kesselheim, M. Sega, and C. Holm, Comput. Phys. Commun. **182**, 33 (2011); Soft Matter **8**, 9480 (2012)
 - [14] Small (large) Debye lengths can be realized by large (small) ion concentrations [12].
 - [15] C. E. Cummings, S. K. Griffiths, R. H. Nilson, and P. H. Paul, Anal. Chem. **72**, 2526 (2000); J. G. Santiago, *ibid.* **73**, 2353 (2001) and further references therein.
 - [16] O. Schnitzer and E. Yariv, Phys. Rev. E **86**, 021503 (2012)
 - [17] As in Ref. [18], we approximate the pore by a hyperboloid with z -dependent pore radius $r(z) = [(d/2)^2 + z^2(D^2 - d^2)/H^2]^{1/2}$ for $|z| \leq H/2$. In addition, the "corners" at $z = \pm H/2$ are rounded (curvature radius 5 nm).
 - [18] S. W. Kowalczyk, A. Y. Grosberg, Y. Rabin, and C. Dekker, Nanotechnology **22**, 315101 (2011)
 - [19] S. H. Behrens and D. G. Grier, J. Chem. Phys. **115**, 6716 (2001); D. Stein, M. Kruithof, and C. Dekker, Phys. Rev. Lett. **93**, 035901 (2004); M. B. Andersen, J. Frey, S. Pennathur, and H. Bruus, J. Colloid Interface Sci. **353**, 301 (2011)
 - [20] J. D. Sherwood, J. Chem. Soc., Faraday Trans. 2, **78**, 1091 (1982)
 - [21] R. F. Probstein, *Physicochemical Hydrodynamics*, Wiley-Interscience, Hoboken, NJ (2003)
 - [22] Y. Ai, J. Liu, B. Zhang, and S. Qian, Anal. Chem. **82**, 8217 (2010)
 - [23] L. Chen and A. T. Conlisk, Biomed. Microdevices **12**, 235 (2010)
 - [24] V. A. Parsegian, Annu. Rev. Biophys. Bioeng. **2**, 221 (1973)
 - [25] S. W. Kowalczyk, D. B. Wells, A. Aksimentiev, and C.

- Dekker, Nano Lett. **12**, 1038 (2012)
- [26] J. D. Jackson, *Classical Electrodynamics*, Wiley, New York (1999)
- [27] A. Parsegian, Nature **221**, 844 (1969); D. J. Bonthuis, J. Zhang, B. Hornblower, J. Mathé, B. I. Shklovskii, and A. Meller, Phys. Rev. Lett. **97**, 128104 (2006)
- [28] Regarding Fig. 6, i.e. in the presence of a membrane gate electrode, one finds that $\Delta\sigma_m \propto \epsilon_m$ (see second to last paragraph). Apart from this rather trivial ϵ_m -dependence, all other effects of ϵ_m and ϵ_p are again very small.
- [29] R. S. Eisenberg, J. Membr. Biol. **150**, 1 (1996); B. Corry, S. Kuyucak, and S. Chung, Biophys. J. **78**, 2364 (2000)
- [30] J. H. Masliyah and S. Bhattacharjee, *Electrokinetic and Colloidal Transport Phenomena*, Wiley, NJ (2006); R. L. Panton, *Incompressible Flow*, Wiley, NJ (2005)
- [31] The numerical solution exploits finite element methods on a triangular grid, properly refined within the Debye layers, and typically involving about 200'000 elements.
- The basis functions are Lagrange shape functions of order one for the pressure and concentration fields, and of order two for the velocity and electric potential fields.
- [32] We found that the potential energy $U(z)$ changes approximately linearly with voltage V up to a few 100 mV.
- [33] D. K. Lubensky and D. R. Nelson, Biophys. J. **77**, 1824 (1999)
- [34] P. C. Yen, C. H. Wang, G. J. Hwang, and Y. C. Chou, Rev. Sci. Instrum. **83**, 034301 (2012); Z. Jiang and D. Stein, Phys. Rev. E **83**, 031203 (2011); S.-W. Nam, M. J. Rooks, K.-B Kim, and S. M. Rossnagel, Nano Lett. **9**, 2044 (2009); M. E. Gracheva, A. Xiong, A. Aksimentiev, K. Schulten, G. Timp, and J.-P. Leburton, Nanotechn. **17**, 622 (2006); B. Luan, H. Peng, S. Polonsky, S. Rossnagel, G. Stolovitzky, and G. Martyna, Phys. Rev. Lett. **104**, 238103 (2010); S. Harrer et al., Nanotechn. **22**, 275304 (2011)